

Effects of High Field Permanent Magnet Insertion Device on the Siam Photon Source Storage Ring

Supagorn Rugmai

School of Physics, Institute of Science, Suranaree University of Technology, 111 University Ave.,
Nakhon Ratchasima 30000, Thailand.
National Synchrotron Research Center, P.O. Box 93, Nakhon Ratchasima 30000, Thailand.

* Corresponding author, E-mail: supagorn@nsrc.or.th

Received 26 Jul 2004
Accepted 4 Feb 2005

ABSTRACT: The Siam Photon Source is a 1 GeV electron storage ring for a synchrotron light source, now under test commissioning in Nakhon Ratchasima, Thailand. The bending magnets of the storage ring produce synchrotron light with photon energy usable up to the soft x-rays regions. In order to extend the usable photon spectrum to higher photon energies an insertion device with high magnetic field has to be installed into the storage ring. This report presents studies of perturbations from the magnetic field of such a device on the electron beam dynamics in the storage ring of the Siam Photon Source. The magnetic field of the device is simulated from arrays of permanent magnets. Random errors of the magnetic structure are included to take into account imperfection of a real device. Effects of perturbations from the magnetic field of the device on the electron beam dynamics are calculated. Possibilities to compensate the perturbations are investigated.

KEYWORDS: synchrotron radiation, insertion device, permanent magnet, storage ring, beam dynamics.

INTRODUCTION

The Siam Photon Source (SPS) is a 1 GeV synchrotron light source¹, now under test commissioning in Nakhon Ratchasima, Thailand. The synchrotron light is emitted from a circulating electron beam, with 1 GeV beam energy, bent by a 1.2 Tesla dipole field of the bending magnets. The synchrotron light emitted from an electron of energy E GeV bent in a magnetic field of B Tesla has a critical photon energy of ²

$$\varepsilon_c = 0.67E^2B \text{ keV.} \quad (1)$$

The bending magnets of the SPS therefore give synchrotron light with the critical photon energy of 0.8 keV. Since the intensity of the synchrotron light with the photon energy above approximately four times the critical photon energy will be too low for practical uses² the bending magnet light from the SPS is naturally utilizable only in the Vacuum Ultra Violet (VUV) and Soft X-rays regions. However, the storage ring of the SPS has been designed to contain four long straight sections, 5.2 meters each, to accommodate insertion devices to be installed at later stages. Insertion devices are a special magnetic device designed to produce synchrotron light with special properties. A wiggler is one type of such devices. It is a magnetic device consisting of high field magnets periodically arranged to produce oscillating magnetic field. The wiggler

functions as multiple bending magnet sources, in which the magnetic field can be made higher than that of the normal bending magnets. The photon energy of the synchrotron light produced by the wiggler can therefore be extended to higher energy regions, depending on the magnetic field of the device. The intensity of the synchrotron light from the wiggler is also higher, being proportional to the number of periods of the oscillating field of the device.

Installing a wiggler into the storage ring is however not a straight forward task. The magnetic field of the wiggler introduces perturbations to the circulating electron beam in the storage ring. Since the magnetic structure of the wiggler consists of arrays of rectangular magnets it possesses intrinsic focusing properties^{3,4}. This focusing results in the vertical tune shift of the electron beam in the storage ring. Moreover, the focusing property of the wiggler produces a spread of resonance lines in the tune diagram, the so-called stop-band. These effects can lead to instability of the electron beam. Effects of these perturbations therefore have to be studied carefully, in order to be effectively compensated to make the storage ring operational after installation of the device.

The magnetic structure of the wiggler can be constructed in various ways. In the past wigglers have mostly been constructed from electromagnets. These electromagnet wigglers however have important disadvantages in that they need large spaces for the

coils of each magnet pole. Most wigglers currently in use are permanent magnet devices. The current permanent magnet technology is able to produce a permanent magnet block, from the magnet material such as Nd-Fe-B, with high remanent field reaching 1.3 Tesla. Such permanent magnet devices have been constructed and operated in many synchrotron light sources^{5,6,7}. The permanent magnet wigglers can produce peak magnetic field reaching high field of 2 Tesla at the magnetic gap of 19 mm with the hybrid design⁸. Development of in-vacuum devices⁹ further helps reducing the magnetic gap for permanent magnet devices, and hence stronger magnetic field. Recent studies have also shown that remanent field of the permanent magnets can be increased by as much as 50% when operating under cryogenic temperature of liquid nitrogen¹⁰. The permanent magnet devices therefore still offer possibility of hard x-rays production for the SPS.

Recently, the superconducting magnet technology has advanced rapidly. This technology is making great contribution to the development of insertion devices. Despite the complexity of having to be operated under cryogenic environment around the liquid helium temperature, the superconducting multipole wigglers have been constructed and developed in many laboratories^{11,12,13}. These superconducting devices are capable of producing very high magnetic field, above 3.5 Tesla. It therefore gives promising possibility for low energy storage rings such as that of the SPS to produce intense synchrotron light in the hard x-rays regions.

In this report the case study will be made with the permanent magnet wiggler. The magnetic field from such a permanent magnet device can be simulated from analytical expressions. It also enables random errors of the magnetic structure to be included to take into account effects of imperfection.

Magnetic Field Simulation

For a permanent magnet wiggler the magnetization direction of the magnet blocks in each array is rotated by 90 degrees from adjacent blocks. This results in the so-called Halbach configuration¹⁴. The magnetic field is then smoothly terminated by adding at both ends of the device the endpoles, with half longitudinal length of the normal poles. The modeled magnetic structure is shown in Figure 1. The structure has asymmetric configuration which has naturally compensated field integral, and which are routinely adopted for insertion devices.

To simulate the magnetic field the magnet arrays can be modeled with uniformly magnetized rectangular permanent magnet blocks. The magnetic field at each point between the two magnet arrays can then be

calculated by superimposing the magnetic field generated by each magnet block. The vertical magnetic field B_y generated by a uniform rectangular magnet block of the width X , height Y and length Z , and with magnetization \vec{M} , can be given analytically by^{15,16}

$$B_y(x,y,z) = \frac{\mu_0 M}{4\pi} [I(X,Y,Z) - I(-X,Y,Z) - I(X,-Y,Z) + I(-X,-Y,Z) - I(X,Y,-Z) + I(-X,Y,-Z) + I(X,-Y,-Z) - I(-X,-Y,-Z)] \quad (2)$$

where, for \vec{M} parallel to the y -axis,

$$I(X,Y,Z) = \tan^{-1} \left[\frac{(X/2-x)(Z/2-z)}{(Y/2-y)\sqrt{(X/2-x)^2 + (Y/2-y)^2 + (Z/2-z)^2}} \right] \quad (3)$$

and for \vec{M} parallel to the x -axis,

$$I(X,Y,Z) = \sinh^{-1} \left[\frac{Z/2-z}{\sqrt{(X/2-x)^2 + (Y/2-y)^2}} \right], \quad (4)$$

where x , y and z denote the horizontal, vertical and longitudinal axes, respectively, with the origin of the coordinate system being at the center of the magnet block. M is the magnitude of the magnetization and μ_0 is the magnetic permeability in vacuum. For \vec{M} parallel to the z -axis, $I(X,Y,Z)$ is given by permutation of $(X/2-x)$ and $(Z/2-z)$. In the case of an arbitrary \vec{M} direction the magnetic field can be calculated by decomposing \vec{M} into components and adding the contributions. The horizontal and longitudinal components of the magnetic field can also be calculated by appropriate permutations of the axes

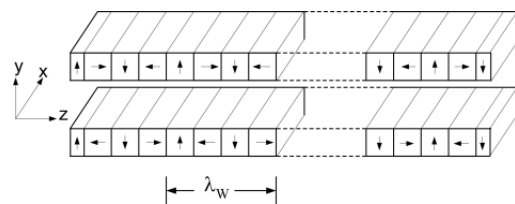


Fig 1. The modeled magnetic structure of the wiggler. The arrows indicate direction of magnetization for each magnet block.

in the expressions.

In the simulation the magnet blocks are assumed to be the Nd-Fe-B magnet. It is commercially available with high uniformity and high remanent field reaching 1.3 Tesla. Recent studies have also shown that permanent field of such permanent magnets can be increased by as much as 50% when operating under cryogenic temperature of liquid nitrogen¹⁰. In order to represent a high field permanent magnet wiggler the remanent field of 1.9 Tesla is therefore assumed in the calculations.

A FORTRAN code has been written to simulate the magnetic field generated by the arrays of rectangular magnet blocks. In practice the magnetic field generated

by a real device cannot be made perfect. The magnetic field errors can arise from various sources, including the magnetic properties of the magnets, the assembling errors and the mechanical errors. With high precision magnetic measurements these errors can be greatly reduced by various methods, such as the sorting or shimming of the magnets^{17,18,19}. Nevertheless, some magnetic errors are inevitable. Here we take into account the remaining small errors by allowing random variation of 1% in the magnetization strength and 1 degree in magnetization direction of each magnet block. In order to obtain the highest possible magnetic field a small magnetic gap is preferred. To avoid restriction of the storage ring vacuum chamber the small gap value can be achieved by making the device in-vacuum⁹. Here the magnetic gap is assumed to be 10 mm.

The sizes of the magnet blocks used to simulate the wiggler field are $X=100$ mm and $Y=45$ mm. These are the smallest sizes where the calculated peak magnetic fields, as a function of magnet block width and height, begin to saturate. The longitudinal dimension of the blocks is related to the period length, i.e. $Z = \lambda_W / 4$, where the period length λ_W is chosen to give the highest peak magnetic field from the device. The period length of 107 mm is obtained from the simulation. The calculated peak magnetic field is 2.21 Tesla, giving the photon critical energy of 1.48 keV. For the simulation, 18 magnetic periods are assumed, resulting in the length of the wiggler of approximately two meters.

Effects of the Wiggler on the Electron Beam Dynamics in the SPS

For installation of insertion devices in a low energy storage ring effects on the electron beam dynamics have to be carefully considered. The wiggler possesses an intrinsic focusing property in the vertical plane, due to the wiggling motion of the electron beam through the oscillating magnetic field. This focusing property gives rise to the change in the betatron tune, the tune shift, of the circulating electron beam in the storage ring. Here we estimate the tune shift due to the presence of the wiggler field in the storage ring using a perturbation method. The wiggler is treated as a thin lens focusing device, inserted at the middle of one of the straight sections of the SPS storage ring.

Since the wiggler is composed of series of rectangular magnets it has the focusing strength being an inverse-square of the radius of curvature of the electron trajectory³. Effects of the focusing of the wiggler may therefore be studied from an averaged focusing strength of the device in the vertical plane,

$$K_y = \left\langle \frac{1}{\rho^2} \right\rangle = \frac{1}{L} \left(\frac{e}{E} \right)^2 \int_{-L/2}^{L/2} B_y^2(z) dz \quad (5)$$

where ρ is the radius of curvature derived from the simulated magnetic field B_y of the wiggler, and L is the magnetic length of the wiggler. In equation (5), e denotes the electron charge. A transfer matrix for such focusing device is therefore

$$M_F = \begin{bmatrix} \cos\sqrt{K_y}L & \frac{1}{\sqrt{K_y}}\sin\sqrt{K_y}L \\ -\sqrt{K_y}\sin\sqrt{K_y}L & \cos\sqrt{K_y}L \end{bmatrix} \quad (6)$$

An effective thin lens acting at the middle of the device can then be constructed by multiplying the focusing matrix from the left and from the right by an inverse of the straight section matrix²⁰,

$$M_{F,eff} = \begin{bmatrix} 1 & -L/2 \\ 0 & 1 \end{bmatrix} M \begin{bmatrix} 1 & -L/2 \\ 0 & 1 \end{bmatrix} \quad (7)$$

The betatron tune shift due to the presence of the device can be found by considering the one-turn matrices of the storage ring with and without the wiggler. The one-turn matrix, in the vertical plane, without the wiggler is given by

$$M_C = \begin{bmatrix} \cos\mu_y + \alpha_y \sin\mu_y & \beta_y \sin\mu_y \\ -\gamma_y \sin\mu_y & \cos\mu_y - \alpha_y \sin\mu_y \end{bmatrix} \quad (8)$$

where $\mu_y / 2\pi$ is the vertical betatron tune, and $\alpha_y, \beta_y, \gamma_y$ are the betatron functions. This unperturbed one-turn matrix can be calculated using the designed low emittance lattice of the SPS storage ring²¹. The vertical one-turn matrix in the presence of the wiggler, treated as a focusing thin lens, is then

$$\begin{bmatrix} \cos\mu_W + \alpha_W \sin\mu_W & \beta_W \sin\mu_W \\ -\gamma_W \sin\mu_W & \cos\mu_W - \alpha_W \sin\mu_W \end{bmatrix} = M_C M_{F,eff} \quad (9)$$

where $\mu_W / 2\pi$ is the vertical betatron tune in the presence of the wiggler. This perturbed betatron tune can be evaluated from the trace of the matrix in Equation (9),

$$\cos\mu_W = \frac{1}{2} \text{Tr}[M_C M_{F,eff}] \quad (10)$$

This therefore leads to the vertical tune shift due to the presence of the wiggler

$$\Delta\nu_y = \frac{\mu_W - \mu_y}{2\pi} \quad (11)$$

In addition to the tune shift, the focusing property of the wiggler also produces a stop-band, a spread of the resonance lines in the tune diagram. If the tune value in the presence of the wiggler falls into the stop-band, the particle motion will become unstable. The stop-band is produced in the condition where the betatron tune does not exist, i.e. $|\cos\mu_W| > 1$. With this condition the stop-band width can readily be calculated from Equation (10). After evaluating the cosine in Equation (10), the result may then be rewritten in the

form

$$\cos\mu_W = a\cos\mu_y - b\sin\mu_y \tag{12}$$

The stop-band condition is therefore

$$(a\cos\mu_y - b\sin\mu_y)^2 > 1, \tag{13}$$

in which the boundaries of the stop-band are given by the solution to the quadratic equation,

$$\tan\mu_y = \frac{ab \pm \sqrt{b^2 + a^2 - 1}}{b^2 - 1}. \tag{14}$$

The Hard-edge Model Wiggler

In order to investigate compensation schemes for restoring the storage ring conditions we need to construct a model of the wiggler for beam dynamics calculations. Here we use the program MAD (Methodical Accelerator Design)²² for such purpose. In this section we first construct such a wiggler model and test the model by confirming the calculated tune shift. The wiggler is modeled in MAD by series of face-rotated sector dipole magnets. However, since dipole magnets are treated in beam dynamic programs as a component having a constant radius of curvature, they cannot represent a correct sinusoidal field characteristic. The magnet poles in the model are therefore modified using the so-called hard-edge magnet to match the deflection angle and the focusing properties of the sinusoidal magnetic field. The radius of curvature for the hard-edge dipole magnet representing each magnet pole is given by³

$$\rho_h = \frac{4}{\pi} \rho_0 \tag{12}$$

and the longitudinal length

$$l_h = \frac{2}{\pi} \lambda_W \tag{13}$$

where ρ_0 is the radius of curvature relating to the peak magnetic field of the wiggler. Such hard-edge model sector dipole magnets are used to model the wiggler in the calculations by MAD, while preserving the overall length of the wiggler.

RESULTS AND DISCUSSION

Calculations of Effects of Perturbations

Having obtained all the parameters for the wiggler the mid-plane, $x=y=0$, vertical magnetic field $B_y(z)$ at the magnetic gap of 10 mm can be simulated. Additionally, following development of permanent magnet insertion devices special end-structures have been proposed in order to correct trajectory offset and minimize field integral variation with the magnetic gap^{9,23}. In the simulation, we adopt the simple structure

proposed by Chavanne et al²³ by placing longitudinally magnetized blocks, having the longitudinal length adjusted to $0.16\lambda_W$, next to the end-poles of the magnetic structure. The simulated magnetic field is shown in Figure 2. The calculated angles and trajectories resulting from such simulated field are shown in Figures 3 and 4, respectively. Effects of random variation can be clearly seen in Figure 4, where the comparison is made with the calculation without the random errors. The errors result in non-zero first and second field integrals. In a real device, however, careful sorting and shimming processes can be expected to give smaller errors. The remaining errors can then be corrected by

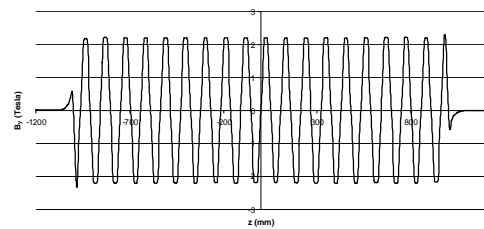


Fig 2. Simulated magnetic field of the modeled wiggler.

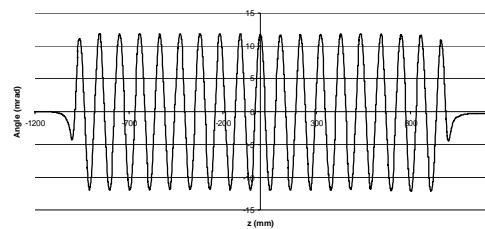


Fig 3. Calculated angles resulting from the simulated magnetic field.

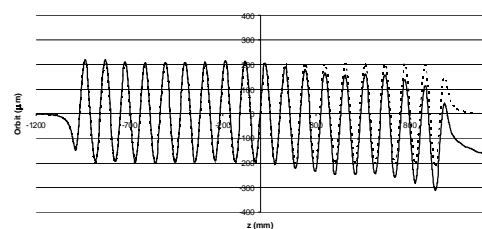


Fig 4. Calculated trajectories resulting from the simulated magnetic field. The broken line shows the calculation without the random errors.

corrector magnets.

The calculated photon flux density from the modeled wiggler is also shown in Figure 5, using the program SPECTRA²⁴, in comparison with that from the bending magnet of the SPS. It is seen that the wiggler significantly increases the photon flux density, particularly in the hard x-rays regions around 10 keV. These regions of hard x-rays are around K-edges of

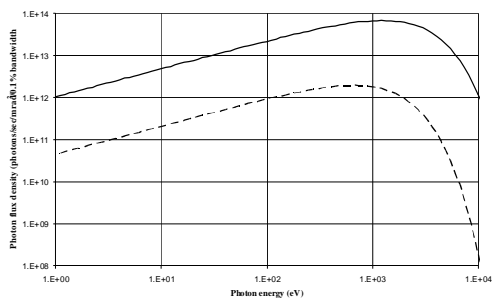


Fig 5. Calculated photon flux density from the modeled wiggler (solid line) and the bending magnet (broken line) of the SPS.

metal elements, and have many important applications.

With the simulated magnetic field the wiggler focusing strength is found from Equation (5) to be 0.124 m^{-2} . Using the unperturbed vertical tune value of $\nu_y = 2.819$ and the vertical betatron functions at the middle of the straight section, being a symmetry point, of $\alpha_y = 0, \beta_y = 3.20 \text{ m}$ and $\gamma_y = 1/\beta_y$, Equation (11) gives the calculated vertical tune shift of 0.057. The stop-band width, calculated from Equation (14), is 0.107. It is seen that the perturbation from the wiggler moves the vertical tune closer to the integer resonance. Taking into account the calculated stop-band width, the perturbed tune is dangerously close to the region of instability.

In the presence of the wiggler the calculations by MAD give the vertical tune shift of 0.058. The obtained value is reasonably close to the value obtained from the simulation above. The result therefore assures the use of the hard-edge model in studies of compensation schemes for the simulated wiggler field.

Compensation of the Perturbations

As seen from the calculations, the perturbations from the wiggler moves the betatron tune of the storage ring. If this perturbed tune crosses a resonance or reaches the stop-band region the electron motion becomes unstable. Moreover, the storage ring of the SPS is designed to be 4-fold symmetric, the presence of the wiggler also naturally destroys the symmetry of the storage ring. Figures 6 and 7 show the calculated beta functions from the electron motion around the storage ring in the absence and the presence of the wiggler, respectively. Breaking of the 4-fold symmetry by the wiggler is clearly seen in Figure 7. Both the tune shift and the asymmetry are not desirable for the operation of the storage ring. Some compensation scheme is therefore needed to restore the symmetry and the operating tune. It is, however, not always possible to completely compensate the effects due to constraints of parameters to be adjusted. Here we investigate possibilities to compensate such perturbations.

We first make an attempt to restore the symmetry of the storage ring. In principle, the focusing effects from the wiggler can be compensated by focusing elements of the storage ring, which are the quadrupole magnets. The SPS storage ring contains 28 quadrupole magnets separated into four families, with the magnets in each family being powered in series by one power supply. Since adjusting an individual quadrupole magnet for compensation requires an additional power supply, an economic constraint has to be part of the consideration. The principle is therefore to compensate the focusing of the wiggler using as few magnets, or sets of magnets, as possible.

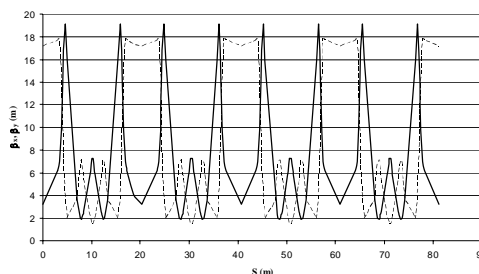


Fig 6. Calculated vertical (solid line) and horizontal (broken line) beta functions for the SPS storage ring, without the wiggler.

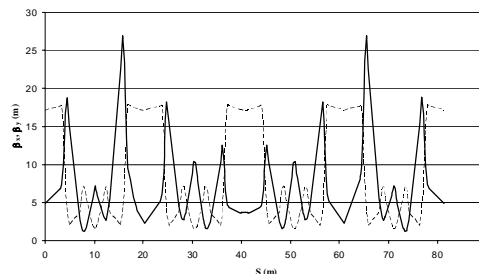


Fig 7. Calculated vertical (solid line) and horizontal (broken line) beta functions for the SPS storage ring, with the wiggler installed at the middle.

We begin with adjusting the strengths of the two pairs of quadrupole magnets, one focusing pair and one defocusing pair, adjacent to the wiggler. The adjusting is carried out using the matching module of MAD to match the perturbed beta functions to the unperturbed ones, leaving the betatron tunes freely variable. It is found from the calculations that the symmetry is restored by increasing the strengths of the focusing quadrupole pair by 0.99% and of the defocusing quadrupole pair by 3.18%. The compensated beta functions are indistinguishable from the unperturbed ones, shown in Figure 6. The vertical betatron tune is moved to $\nu_y = 2.932$, while the

horizontal tune remains unchanged at $\nu_x = 4.748$.

The result from the beta function matching is, however, not satisfactory. Despite the symmetry being restored, the new vertical tune is dangerously close to the integer resonance. We next investigate the betatron tune matching. Using similar procedure, but the quadrupole strengths are now adjusted to match the perturbed betatron tunes to the unperturbed values. It is noted that since adjusting the strengths of the quadrupole magnets disturbs the electron motion in both planes, the horizontal tune has to be included in the matching constraints. From the calculations, by decreasing the strengths of the focusing quadrupole pair by 1.23% and of the defocusing quadrupole pair by 4.56% the vertical and horizontal tune shifts are kept to within $\Delta\nu_y = 0.004$ and $\Delta\nu_x = 0.003$, respectively. In this case, however, the symmetry of the storage ring is still broken badly, as shown in Figure 8.

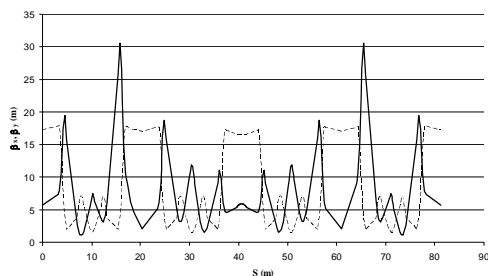


Fig 8. Calculated vertical (solid line) and horizontal (broken line) beta functions for the SPS storage ring, with the wiggler. The betatron tunes are fitted to the unperturbed values.

At the last step we make an attempt to compromise between restoring the symmetry and the betatron tunes. This matching is carried out by allowing additional two further pairs of quadrupole magnets, one focusing pair and one defocusing pair, adjacent to the two previous pairs, to be adjusted. It is, however, found to be difficult to achieve the perfect compensation. The best result obtained is by increasing the strengths of the first quadrupole pair by 0.74%, decreasing the second pair by 0.23%, decreasing the third pair by 0.13% and decreasing the fourth pair by 8.60%. This compensation scheme keeps the betatron tune shifts to within $\Delta\nu_y = 0.009$ and $\Delta\nu_x = 0.004$. The symmetry is, however, not perfectly restored, as shown in Figure 9. Nevertheless, the storage ring is expected to be operational in this condition. Other possibilities for compensation may be further investigated. This includes moving the operation tunes to other values altogether, which will give more flexibility for compensation. Another option is to install additional quadrupole magnets at both ends of the wigglers. These

options, however, need further comprehensive studies. Furthermore, in a real device there will be small contributions from additional multipole field components arising from imperfection of the magnetic arrangement and inhomogeneous field distribution within the magnets. These small multipole components can be accurately identified via high precision magnetic measurements. More detailed studies can then be carried out to compensate such errors.

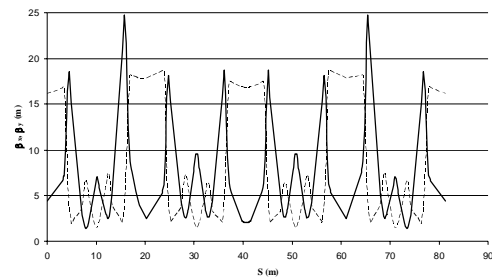


Fig 9. Calculated vertical (solid line) and horizontal (broken line) beta functions for the SPS storage ring, with the wiggler. The betatron tunes and beta functions are fitted to the unperturbed values.

CONCLUSIONS

We have presented a case study of effects of a high field insertion device on the SPS storage ring. The oscillating magnetic field of the device is simulated from series of permanent magnets, allowing random errors of the magnetization. The wiggler focusing strength is calculated from the simulated magnetic field. The vertical betatron tune shift and stop-band width resulting from perturbations of the wiggler are evaluated and found significant. Compensation schemes to restore the storage ring symmetry and correct the tune shift are presented. The studies carried out in this report can be easily applied to other types of insertion devices to be installed in the SPS in the future.

ACKNOWLEDGEMENTS

The author is grateful to Professor H. Wiedemann (Stanford University) for invaluable discussion and advice on beam dynamics calculations, and to S. Chunjarean (National Synchrotron Research Center) for help on the MAD program.

REFERENCES

1. Songsirithikul P, Pairuwan W, Jearanaikul S and Ishii T (1999) The Siam Photon Source. *Suranaree J. Sci. Technol.* **6**, 22-

- 31.
2. Wiedemann H (1995) *Particle Accelerator Physics I*. Springer-Verlag, Berlin.
3. Wiedemann H (1995) *Particle Accelerator Physics II*. Springer-Verlag, Berlin.
4. Walker RP (1995) Wigglers. In: *Cern Accelerator School Proceedings*, pp 807-35.
5. Kitamura H (1998) Present status of SPring-8 insertion devices. *J. Synchrotron Rad* **5**, 184-8.
6. Gluskin E (1998) APS insertion devices: recent development and results. *J. Synchrotron Rad* **5**, 189-95.
7. Chavanne J, Elleaume P and Vaerenbergh PV (1998) The ESRF insertion devices. *J. Synchrotron Rad* **5**, 196-201.
8. Clarke JA and Dobbins GS (1999) Commissioning of the new multipole wiggler in the SRS. *Proceedings of the Particle Accelerator Conference*, pp 2653-5.
9. Hara T, Tanaka T, Tanabe T, Marechal XM, Okada S and Kitamura H (1998) In-vacuum undulator for Spring-8. *J. Synchrotron Rad* **5**, 403-5.
10. Hara T, Tanaka T and Kitamura H (2004) Cryogenic permanent magnet undulators. *Phys. Rev. ST. Acc. Beams*. **7**, 050702-1-6.
11. Batrakov A *et al* (2001) Superconducting wavelength shifters and multipole wigglers developed in Budker INP. *Proceedings of the Second Asian Particle Accelerator Conference*, pp 251-3.
12. Batrakov A *et al* (2002) A superconducting 3.5 T multipole wiggler for the ELETTRA storage ring. *Proceeding of European Particle Accelerator Conference*, pp 2634-6.
13. Fan TC, Lin FY, Huang MH, Chang CH and Wang CS (2003) Magnetic field measurement on superconducting multipole wiggler with narrow duct. *Proceedings of the Particle Accelerator Conference*, pp 1047-9.
14. Halbach K (1981) Physical and optical properties of rare earth cobalt magnets. *Nucl. Instr. Meth.* **187**, 109-17.
15. Ortega JM, Bazin C, Deacon DAG, Depautes C and Elleaume P (1983) Realization of the permanent magnet undulator NOEL. *Nucl. Instr. Meth.* **206**, 281-8.
16. Marechal XM, Chavanne J and Elleaume P (1990) Magnetic field generated by parallelepiped permanent magnet block. *European Synchrotron Radiation Facility Technical Notes ESRF-SR/ID-90-37*.
17. Tanaka T and Kitamura H (2000) Effective initial sorting of undulator magnets. *Rev. Sci. Instr.* **71**, 1-6.
18. Chavanne J, Chinchio E and Elleaume P (1989) New techniques for development of high quality undulators for synchrotron sources. *European Synchrotron Radiation Facility Technical Notes ESRF-SR/ID-89-27*.
19. Chavanne J, Elleaume P and Revol F (1989) Analysis of magnetization mechanisms inside shims. *European Synchrotron Radiation Facility Technical Notes ESRF-SR/ID-89-32*.
20. Bassetti M, Cattoni A, Luccio A, Preger M and Tazzari S (1977) A transverse wiggler magnet for ADONE. *Laboratori Nazionali Frascati Technical Notes LNF-77/26(R)*.
21. Chunjarean S (2004) Low emittance study for 1.4 GeV SPS storage ring. *National Synchrotron Research Center Technical Notes NSRC-TN-2004/07*.
22. Grote H and Iselin FC (1996) The MAD program (Methodical Accelerator Design) Version 8.19. *CERN/SL/90-13 (AP) (Rev.5)*.
23. Chavanne J, Elleaume P and Vaerenbergh PV (1999) End field structure for linear/helical insertion devices. *Proceedings of the Particle Accelerator Conference*, pp 2665-7.
24. Tanaka T and Kitamura H (2001) SPECTRA : a synchrotron radiation calculation code. *J. Synchrotron Rad* **8**, 1221-8.